Title
Conserved SUN-KASH Interfaces Mediate LINC Complex-Dependent Nuclear Movement and Positioning

Journal
Current Biology, 28(19)

ISSN
0960-9822

Authors
Cain, Natalie E
Jahed, Zeinab
Schoenhofen, Amy
et al.

Publication Date
2018-10-01

DOI
10.1016/j.cub.2018.08.001

Peer reviewed

Article

Current Biology

Conserved SUN-KASH Interfaces Mediate LINC Complex-Dependent Nuclear Movement and Positioning

Graphical Abstract

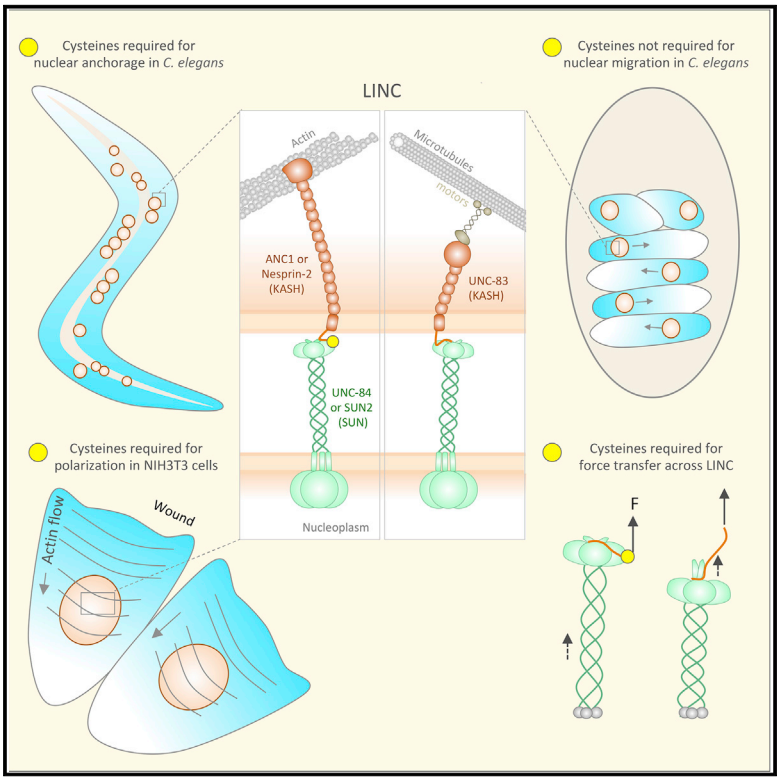

Authors

Natalie E. Cain, Zeinab Jahed, Amy Schoenhofen, ..., Mohammad R.K. Mofrad, G.W. Gant Luxton, Daniel A. Starr

Correspondence

dastarr@ucdavis.edu

In Brief

Cain et al. test the function of mutant SUN and KASH proteins in *C. elegans* nuclear positioning, NIH 3T3 fibroblast polarization, and simulations of LINC complexes under mechanical strain to gain mechanistic insights into how SUN-KASH interactions might be regulated to transfer forces from the cytoskeleton to the nucleus.

Highlights

- Mutating conserved residues at SUN-KASH interfaces disrupts LINC function
- Cysteines in LINC are required to anchor, but not to move, *C. elegans* nuclei
- Cysteines in LINC are needed for nuclear movement in wound-edge fibroblasts
- Simulations show disulfide bridges maximize forces transferred across LINC

Cain et al., 2018, Current Biology *28*, 3086–3097
October 8, 2018
https://doi.org/10.1016/j.cub.2018.08.001

CellPress

CellPress

Current Biology
Article

Conserved SUN-KASH Interfaces Mediate LINC Complex-Dependent Nuclear Movement and Positioning

Natalie E. Cain,[1] Zeinab Jahed,[2] Amy Schoenhofen,[3] Venecia A. Valdez,[1] Baila Elkin,[3] Hongyan Hao,[1] Nathan J. Harris,[3] Leslie A. Herrera,[1] Brian M. Woolums,[3] Mohammad R.K. Mofrad,[2] G.W. Gant Luxton,[3] and Daniel A. Starr,[1,4,*]
[1]Department of Molecular and Cellular Biology, University of California, Davis, 1 Shields Avenue, Davis, CA 95616, USA
[2]Molecular Cell Biomechanics Laboratory, Departments of Bioengineering and Mechanical Engineering, University of California, Berkeley, 208A Stanley Hall, Berkeley, CA 94720, USA
[3]Department of Genetics, Cell Biology, and Development, University of Minnesota, 420 Washington Avenue SE, Minneapolis, MN 55455, USA
[4]Lead Contact
*Correspondence: dastarr@ucdavis.edu
https://doi.org/10.1016/j.cub.2018.08.001

SUMMARY

Many nuclear positioning events involve linker of nucleoskeleton and cytoskeleton (LINC) complexes, which transmit forces generated by the cytoskeleton across the nuclear envelope. LINC complexes are formed by trans-luminal interactions between inner nuclear membrane SUN proteins and outer nuclear membrane KASH proteins, but how these interactions are regulated is poorly understood. We combine *in vivo C. elegans* genetics, *in vitro* wounded fibroblast polarization, and *in silico* molecular dynamics simulations to elucidate mechanisms of LINC complexes. The extension of the KASH domain by a single alanine residue or the mutation of the conserved tyrosine at −7 completely blocked the nuclear migration function of *C. elegans* UNC-83. Analogous mutations at −7 of mouse nesprin-2 disrupted rearward nuclear movements in NIH 3T3 cells, but did not disrupt ANC-1 in nuclear anchorage. Furthermore, conserved cysteines predicted to form a disulfide bond between SUN and KASH proteins are important for the function of certain LINC complexes, and might promote a developmental switch between nuclear migration and nuclear anchorage. Mutations of conserved cysteines in SUN or KASH disrupted ANC-1-dependent nuclear anchorage in *C. elegans* and Nesprin-2G-dependent nuclear movements in polarizing fibroblasts. However, the SUN cysteine mutation did not disrupt nuclear migration. Moreover, molecular dynamics simulations showed that a disulfide bond is necessary for the maximal transmission of cytoskeleton-generated forces by LINC complexes *in silico*. Thus, we have demonstrated functions for SUN-KASH binding interfaces, including a predicted intermolecular disulfide bond, as mechanistic determinants of nuclear positioning that may represent targets for regulation.

INTRODUCTION

The precise intracellular positioning of the nucleus is essential for many cellular and developmental processes including fertilization, cell migration, cell polarization, gametogenesis, neuronal development, and muscle development. Defects in nuclear positioning result in developmental disorders in tissues, including the central nervous system, reproductive organs, and skeletal muscle [1–4]. Most nuclei are positioned by the cytoskeleton, which is physically coupled to the nuclear envelope via a conserved nuclear envelope-spanning molecular bridge known as the linker of nucleoskeleton and cytoskeleton (LINC) complex [5].

The LINC complex is formed by a trans-luminal direct interaction between Sad1/UNC-84 (SUN) proteins in the inner nuclear membrane and Klarsicht/ANC-1/Syne homology (KASH) proteins spanning the outer nuclear membrane (Figure 1) [7–10]. SUN proteins contain a conserved KASH protein-binding luminal C-terminal SUN domain [11] and divergent N termini that interact with lamins and chromatin within the nucleoplasm [9, 12, 13]. KASH proteins contain a conserved C-terminal KASH domain, comprising a trans-membrane domain followed by the ~10- to 32-residue luminal KASH peptide [14]. The divergent N termini of KASH proteins extend into the cytoplasm and engage the cytoskeleton [5, 15, 16]. Thus, LINC complexes enable force transmission across the nuclear envelope [5, 15].

Crystal structures of mammalian SUN2 in complex with KASH peptides from Nesprin-1 or -2 provide insights into the molecular mechanisms of LINC complex-dependent mechanotransmission and nuclear positioning [6, 17]. The structures predict that SUN2 functions as a homo-trimer where each protomer consists of a non-conventional coiled-coil region followed by a β sandwich core with an ~20-residue β hairpin extension, known as the KASH lid. Three independent KASH peptides interact with a single SUN2 homo-trimer [6, 17]. Our recent studies show that the luminal domain of SUN2 does homo-trimerize in living cells [18, 19].

Each KASH peptide forms three binding interfaces with a SUN trimer (Figure 1C) [6, 20]. First, the last four residues of KASH proteins (0 to −3; gray in Figure 1C), consisting of the PPPX motif, fit into a binding pocket formed primarily by a single SUN protomer (P1; green in Figure 1C). Second, positions −4 to −14 of KASH

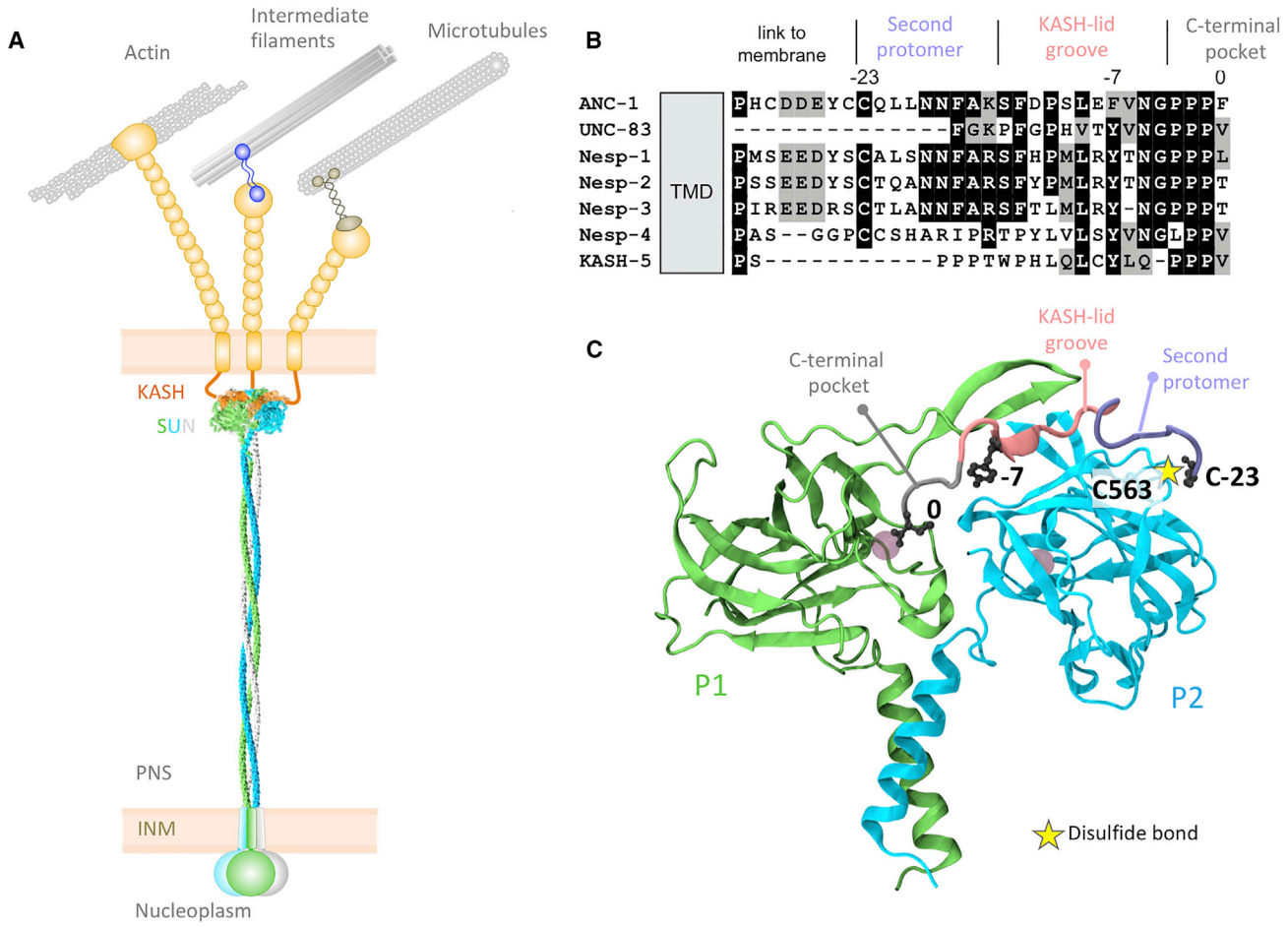

Figure 1. SUN and KASH Proteins Form a Bridge across the Nuclear Envelope

(A) SUN trimers (gray, blue, and green) cross the inner nuclear membrane (INM) and span most of the perinuclear space (PNS). SUN proteins interact with the luminal domains of KASH proteins (orange and tan), extending from the outer nuclear membrane (ONM). Cytoplasmic domains of KASH proteins interact with a variety of cytoskeletal components.

(B) Sequence alignment of *C. elegans* and human KASH domains.

(C) A close-up of the interaction between a KASH peptide (Nesprin-2; gray, pink, and purple) and two SUN2 protomers (green and blue). The gray circles in the SUN protomers represent cations. Based on PDB: 4DXS [6].

proteins (pink in Figure 1C) fit into a groove between two SUN protomers (P1 and P2), with the conserved hydrophobic residues at −7 and −9 facing into the cleft between P1 and P2. Third, residues −15 to −23 (purple in Figure 1C) bind along the surface of P2. At position −23 of the KASH peptide, a conserved cysteine is oriented to form a disulfide bond (yellow star in Figure 1C) with a conserved cysteine in SUN2 (C563 in human SUN2, C577 in mouse SUN2, and C953 in *C. elegans* UNC-84) [20]. Furthermore, an intermolecular disulfide bond was detected between transiently expressed SUN and KASH domains in HeLa cells [6, 20]. Although this covalent bridge was determined by *in vitro* pull-downs to be dispensable for the SUN2-KASH interaction, it was hypothesized to be important for LINC complexes to resist the considerable cytoskeleton-generated forces necessary for nuclear positioning [6, 20]. However, the physiological relevance of each of the three conserved SUN-KASH interaction domains and the conserved disulfide bond during intracellular nuclear movement and positioning remains to be tested experimentally. Here, we examine the effect of disrupting SUN-KASH interactions in two established experimental assays for intracellular nuclear positioning: nuclear migration and anchorage in developing *C. elegans* hypodermal cells [21, 22], and rearward nuclear positioning during centrosome orientation in migrating fibroblasts [23–25]. Furthermore, we used molecular dynamics simulations of SUN2-KASH complexes under tension to model how disrupting SUN-KASH interactions might influence the ability of LINC complexes to withstand the mechanical forces required for nuclear positioning.

Nuclear positioning in *C. elegans* consists of two related processes—nuclear migration to a specific location and then anchoring in place. Nuclear migration in hyp7 precursors requires the SUN protein UNC-84 and the KASH protein UNC-83, which recruit microtubule motors to the surface of nuclei [11, 26, 27]. After the hyp7 syncytium is formed, UNC-84 and the KASH protein ANC-1 anchor nuclei to the actin cytoskeleton [11, 14]. In mammals, KASH proteins Nesprin-4 and KASH5 play

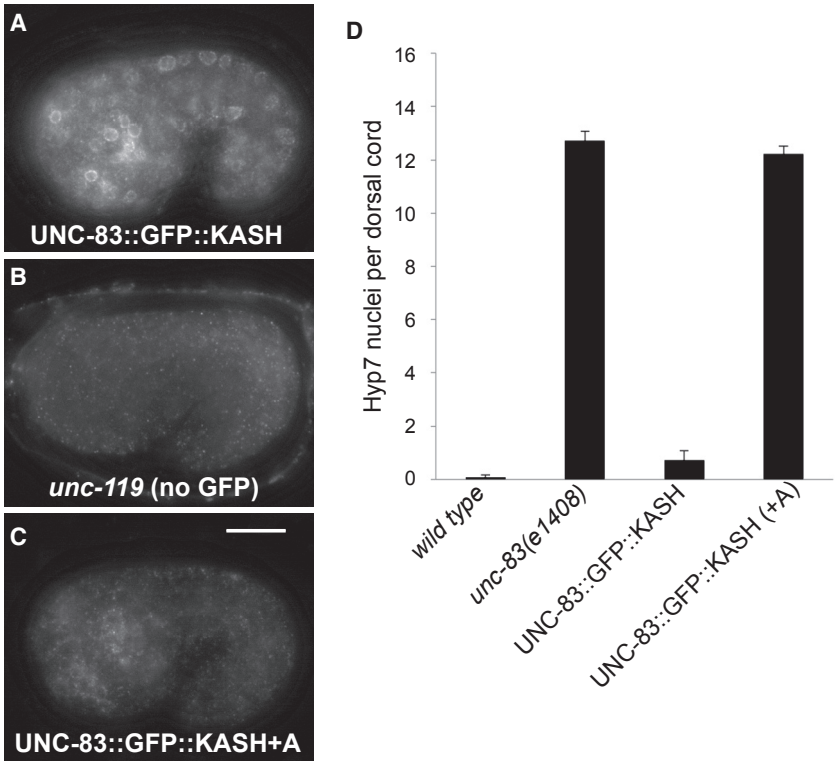

Figure 2. Extension of the KASH Domain of UNC-83 Blocks Nuclear Migration

(A–C) GFP expression in comma-stage embryos with the version of UNC-83 indicated. Anterior is left; dorsal is up. Scale bar, 10 μm.

(A) UNC-83::GFP::KASH.

(B) *unc-119*, which serves as the wild-type UNC-83 (no GFP) control.

(C) UNC-83::GFP::KASH+A.

(D) Quantification of nuclear migration defects by counting the average number of hyp7 nuclei in the dorsal cords of larval stage (L)1 animals. Error bars are 95% CI.

analogous roles recruiting microtubule motors to the surface of nuclei [28, 29]. In other mammalian cell types, giant isoforms of Nesprin-1 and -2 tether mammalian nuclei to actin networks [30–32]. However, it remains unknown how UNC-84-UNC-83 complexes that move nuclei eventually yield to UNC-84-ANC-1 complexes to mediate nuclear anchorage. Interestingly, the KASH domain in UNC-83 is much shorter than in ANC-1; the UNC-83 perinuclear luminal domain is only 17 residues and lacks the cysteine at −23 (Figure 1B) [7]. We hypothesized that an intermolecular disulfide bond formed between conserved cysteines at −23 of KASH peptides and at 563 of human SUN2 (residue 577 of mouse SUN2) or 953 of *C. elegans* UNC-84 plays a central role in LINC complex function. In order to elucidate potential molecular mechanisms for LINC complex regulation, we addressed the following. How important is the interaction between conserved residues in SUN and the PPPX motif of KASH? What happens when the interaction between the aromatic residue at the −7 position of KASH and the cleft between P1 and P2 is disrupted? And, what is the physiological relevance of the disulfide bond between SUN and KASH domains?

RESULTS

Extension of the C Terminus of the UNC-83 KASH Domain Disrupts Nuclear Migration *In Vivo*

The crystal structures of mammalian SUN-KASH complexes show the C terminus of KASH pointed into the SUN protomer P1, where it is coordinated by conserved hydroxyl groups [6, 17] (Figure 1C). Furthermore, the addition of a single alanine to the end of KASH peptides was shown to abolish *in vitro* pull-down interactions between SUN2 and KASH [6], whereas the extension of KASH peptides by 13 residues blocks their function in binding assays and acts as a dominant-negative construct in tissue-culture cells [33]. Therefore, we predicted that the extension of the KASH domain of UNC-83 by one residue would disrupt the interaction between UNC-84 and UNC-83 and disrupt nuclear migration *in vivo*. We used UNC-83::GFP::KASH, which has normal function for nuclear migration [34], as a starting point (Figures 2A and 2D) and added a single alanine onto the C terminus of UNC-83 to express UNC-83::GFP::KASH+A at endogenous levels. UNC-83::GFP::KASH+A failed to localize to the nuclear envelope, similar to when the entire KASH domain of UNC-83 was deleted [7]. As a control, we measured the relative fluorescence in the GFP channel in a standardized region of interest. UNC-83::GFP::KASH+A had 48.7 ± 7.6 (mean ± SD) arbitrary units of fluorescence per embryo compared to 27.1 ± 6.5 arbitrary units in wild-type embryos (t test; $p < 0.0001$), suggesting that the UNC-83::GFP::KASH+A construct was expressed but failed to localize to the nuclear envelope. The resulting animal had a severe nuclear migration defect (Figures 2C and 2D). Thus, the KASH+A mutation blocks SUN-KASH function *in vivo*.

Mutation of the Tyrosine at –7 of KASH Disrupts SUN-KASH Function *In Vivo*

Residues −5 to −14 of KASH proteins (pink in Figure 1) fit into a cleft between two SUN protomers. The conserved hydrophobic aromatic residue at −7 faces directly into the cleft in the crystal structure and a KASH(Y-7A) mutation blocked SUN2-KASH interactions *in vitro* [6]. Overexpressed mutant UNC-83(Y-7A) in a transgenic animal localized to the nuclear envelope, but did not rescue *unc-83(null)* nuclear migration defects [7]. To rule out the effects of overexpression and test the role of Y-7 more directly, we used CRISPR/Cas9 genome editing to introduce the Y-7A mutation into the *unc-83* locus. The resulting *unc-83(Y-7A)* mutant animal completely blocked nuclear migration in hyp7 cells (Figures 3A–3E). However, UNC-83(Y-7A) localized normally to the nuclear envelope of hyp7 cells (Figures 3C and 3D), suggesting that unlike UNC-83(KASH+A), the UNC-83(Y-7A) mutant protein can partially interact with the SUN domain of UNC-84 for localization but that the interaction fails to withstand forces across the nuclear envelope required to move nuclei in these cells.

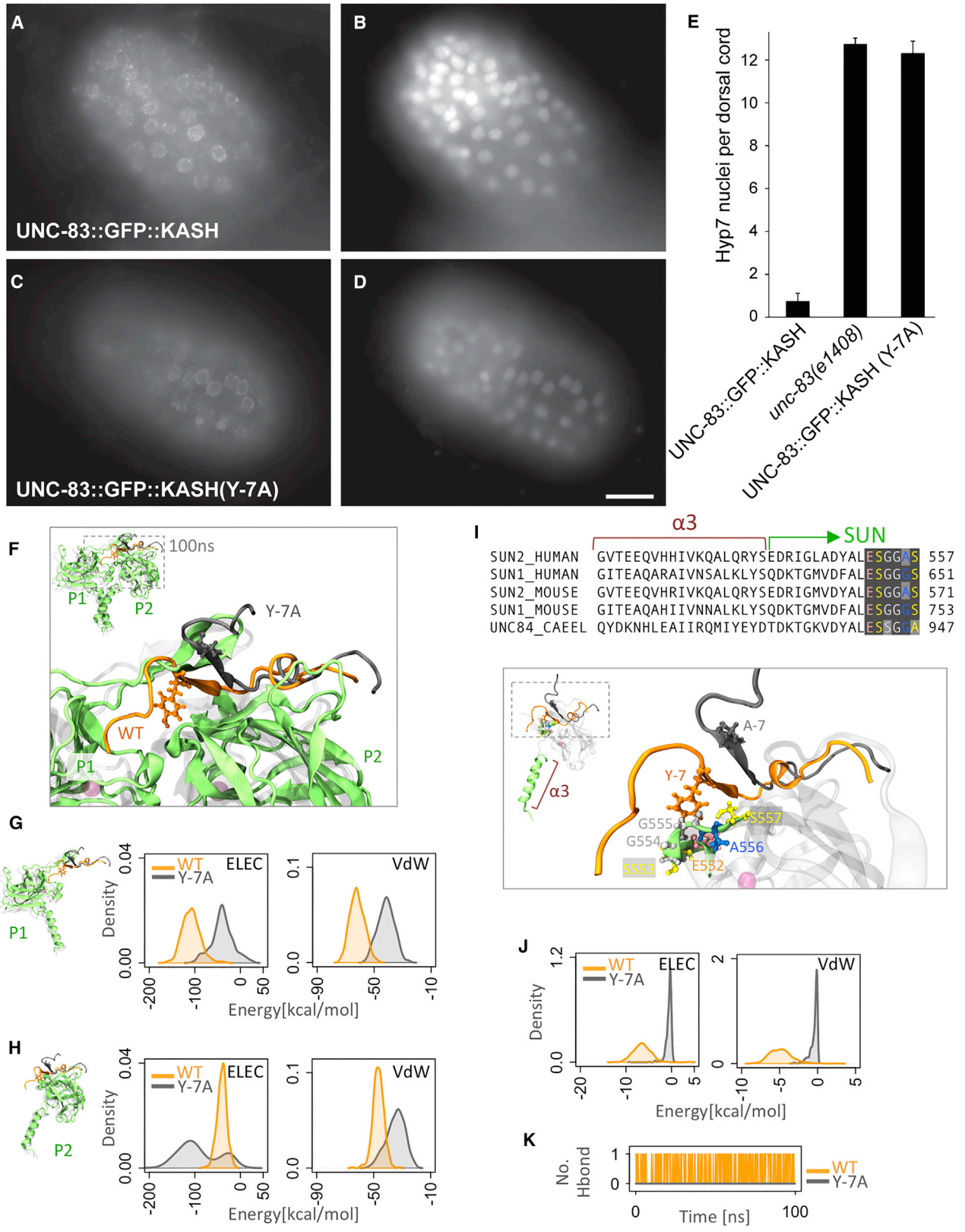

Figure 3. Mutation of Tyrosine –7 of KASH Disrupts SUN-KASH Interactions

(A–D) Anti-GFP immunolocalization (A and C) and DAPI staining (B and D) in pre-bean embryos around the time of hyp7 nuclear migration. Scale bar, 10 μm.

(E) Quantification of nuclear migration defects as in Figure 2. Error bars are 95% CI.

(legend continued on next page)

We used molecular dynamics simulations to examine the extent to which the KASH(Y-7A) mutation might compromise SUN-KASH interactions. We performed simulations of the human SUN2 trimer bound to wild-type Nesprin-2 or Nesprin-2(Y-7A) KASH peptides. Within 100 ns of simulation time, the KASH(Y-7A) peptides partially detached from the SUN2 trimer (Figure 3F). We calculated the non-bonded interaction energies between the KASH(Y-7A) peptide and P1 or P2 over the 100-ns simulation and compared it with wild-type (Figures 3G and 3H). Because the KASH domain of UNC-83 only contains residues 0 to −17, we included the analogous 18 residues of the Nesprin-2 KASH peptide in our energy calculations. The van der Waals (VdW) and electrostatic (ELEC) interactions between the 17 residues of KASH(Y-7A) and P1 were significantly reduced compared with wild-type (Figure 3G). Because the KASH(Y-7A) peptide was partially released from P1, it attempted to form new ELEC contacts with P2 during the simulation time before it partially detached from P2 as well (hence the two peaks in the density of ELEC energies of KASH(Y-7A) with P2 in Figure 3H). Note that the KASH(Y-7A) peptide did not fully detach from P1 or P2 during our simulation (Figures 3G and 3H), which supports our *in vivo* data. We further examined SUN-KASH crystal structures to identify the main interacting partners of SUN2 for the tyrosine at −7 of KASH. The side chain of tyrosine −7 reaches into the trimer and interacts with a highly conserved motif of SUN2 (E552–S557) in P2 (Figure 3I). An alanine at position −7 is not able to reach this motif. To verify this, we computed the non-bonded interaction energies between the residue at position −7 and the E552–S557 motif in P2. This interaction was completely lost with the KASH(Y-7A) mutation (Figure 3J). Additionally, a hydrogen bond between tyrosine −7 of KASH and the E552–S557 motif was lost in simulations with the Y-7A mutation (Figure 3K). Thus, these simulations support *in vivo* data that the tyrosine at −7 of KASH is necessary to transfer forces across the nuclear envelope.

The Cysteine at –23 of the ANC-1 KASH Domain Is Required for Nuclear Anchorage

Residues −15 to −23 of KASH peptides (purple in Figure 1) traverse along the surface of P2 before they disengage from SUN proteins and extend toward the outer nuclear membrane. This interaction domain has been proposed to stabilize LINC complexes and allow for maximal force to be transferred across the nuclear envelope [35]. We hypothesized that mutating the conserved cysteine at −23 of the KASH domain of ANC-1 would disrupt nuclear anchorage in *C. elegans*.

Previous assays for nuclear anchorage defects were qualitative and tended to overestimate anchorage defects [11, 36]. To quantify nuclear anchorage, we expressed nuclear GFP in adult syncytial hypodermal cells. In wild-type young adults, an average of 2.4% ± 1.3% (mean ± 95% confidence interval [CI]) GFP-positive nuclei per lateral side of an animal were clustered (Figures 4A and 4H). In contrast, an *anc-1(e1873)* null animal had an average of 57.3% ± 6.1% ($p < 0.0001$ in a t test) clustered nuclei per lateral side (Figures 4B and 4H). Also, ANC-1 nuclei appear smaller and misshapen. Surprisingly, this assay showed that *unc-84(n369)* null animals have a much less severe nuclear anchorage defect, with only 26.5% ± 5.3% clustered nuclei per lateral side ($p < 0.0001$ in a t test compared to wild-type or *anc-1(e1873)*) (Figures 4C and 4H). This suggests that ANC-1 functions to anchor nuclei through at least two pathways—one through UNC-84 and a second, KASH-independent pathway that will require future investigation.

To test the contribution of the cysteine at −23 of the ANC-1 KASH domain to nuclear anchorage, we edited the conserved cysteine at −23 of the ANC-1 KASH domain and an unconserved cysteine at −24 (Figure 1B) to alanines to make *anc-1(CC-23,-24AA)*. The double-cysteine mutant had a significant nuclear anchorage defect of 11.3% ± 6.0% clustered nuclei ($p < 0.0001$ in a t test compared to wild-type) (Figures 4D and 4H). Thus, the cysteines near −23 of ANC-1 are necessary for normal anchoring of nuclei.

The Cysteine at 953 of the SUN Domain of UNC-84 Is Required for Nuclear Anchorage but Dispensable for Nuclear Migration

Although ANC-1 has a full-length KASH domain with the conserved cysteine at −23, UNC-83 lacks the third interaction domain and connects from residue −18 directly to the transmembrane domain [7]. We therefore hypothesized that an intermolecular disulfide bridge between SUN and KASH would be dispensable for nuclear migration but needed for nuclear anchorage. Genome editing was used to make *unc-84::gfp(C953A)*. We previously reported that the CRISPR/Cas9-edited strain *unc-84::gfp* is functional (Figures 3E, 3H, 5B, and 5C) [37]. In two independent lines, UNC-84::GFP(C953A) localized in a pattern indistinguishable from otherwise wild-type UNC-84::GFP (Figures 5A and 5C), recruited UNC-83 to the nuclear envelope (Figures 5B and 5D), and displayed nearly normal levels of nuclear migration (Figure 5E). In contrast, *unc-84::gfp(C953A)* mutant animals had significant nuclear anchorage defects with 16.2% ± 4.0% and 17.2% ± 2.6% clustered nuclei per lateral side of an adult ($p < 0.0001$ compared to UNC-84::GFP for both t tests) (Figures 4F–4H). We conclude that the conserved cysteine at 953 of UNC-84 is dispensable for nuclear migration but required for normal nuclear anchorage.

(F–K) Modeling the effect of Y-7A on SUN-KASH interactions.

(F) Superimposed structures of wild-type (orange) and Y-7A (gray) after 100 ns of molecular dynamics simulation time. Only two of three SUN2 protomers are shown (P1 and P2).

(G and H) Electrostatic (ELEC) and van der Waals (VdW) energies between KASH (residues 0 to −17) and the P1 (G) or P2 (H) SUN2 protomer for wild-type (WT) (orange) and Y-7A (gray) (shown as densities over a 100-ns simulation time).

(I) Sequence and structure of α3 and the first few residues of the SUN domain showing that the major interacting partners of Y-7 on SUN P2 (E552–S557) are highly conserved.

(J) ELEC and VdW energies between residue −7 and residues E552–S557 on SUN2 P2 for wild-type (orange) and Y-7A (gray) (shown as densities over a 100-ns simulation time).

(K) Number of H bonds between residue −7 and residues E552–S557 on SUN2 P2 for wild-type (orange) and Y-7A (gray).

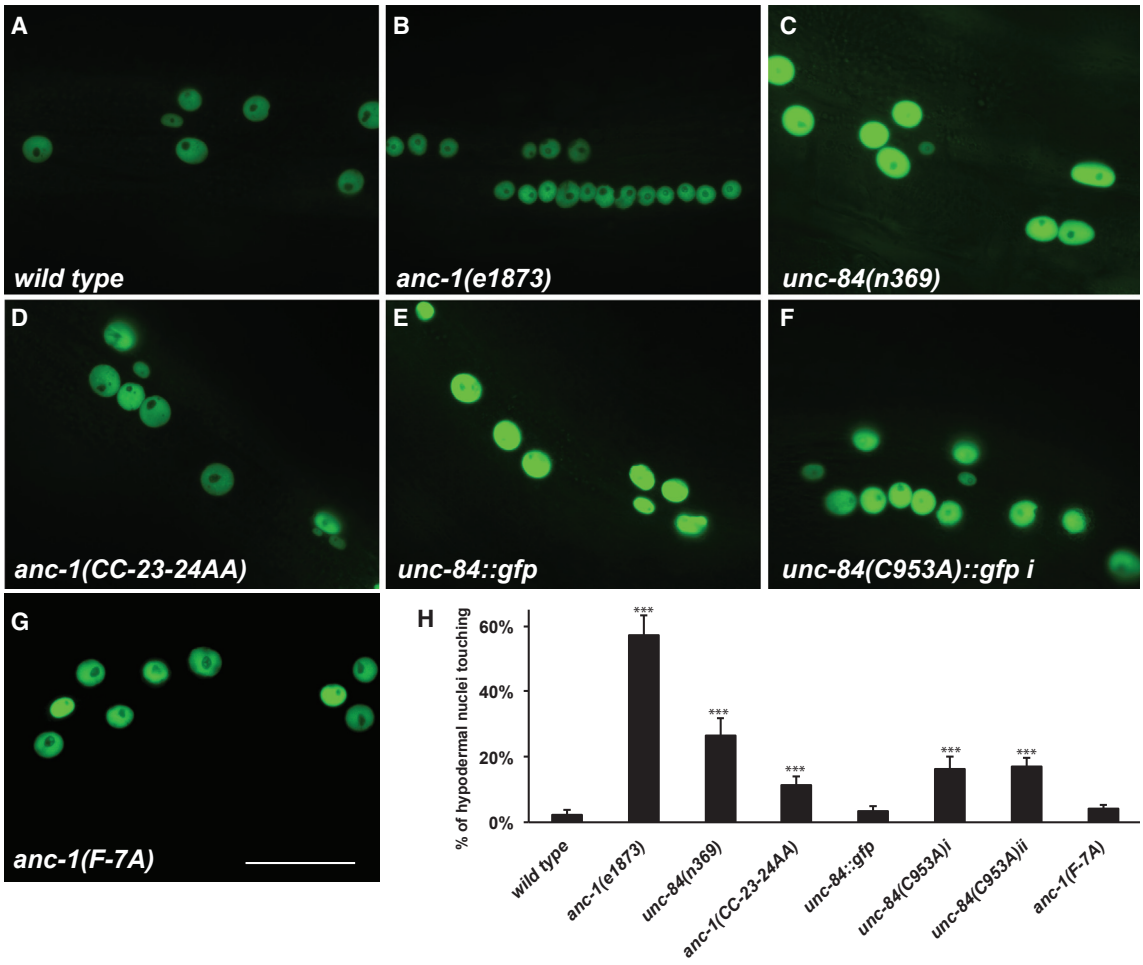

Figure 4. Mutating Conserved Cysteines in UNC-84 or ANC-1 Disrupts Nuclear Anchorage

(A–G) Lateral views of L4 or young adult animals expressing GFP in hypodermal nuclei in the following genotypes: (A) wild-type; (B) *anc-1(e1873)*; (C) *unc-84(n369)*; (D) *anc-1(CC-23-24AA)*; (E) *unc-84::gfp*; (F) *unc-84(C953A)::gfp* line I; and (G) *anc-1(F-7A)*. Scale bar, 25 μm.

(H) Quantification of nuclear anchorage defects assayed by counting the average number of hypodermal nuclei in clusters of two or more nuclei on one lateral side of an animal. Error bars are 95% CI; ***p < 0.0001 in a t test when compared to wild-type; all sample sizes are ≥20 animals.

Cysteines 577 of Mouse SUN2 and –23 of Nesprin-2 Are Required for Rearward Nuclear Positioning in Migrating NIH 3T3 Fibroblasts

Our results in *C. elegans* are consistent with a role for a covalent link between UNC-84 and ANC-1 in nuclear anchoring. We next tested whether a similar role could be observed during mammalian nuclear positioning. Actin-dependent rearward nuclear positioning in wounded monolayers of fibroblasts polarizing for migration is an established assay for LINC complex-dependent nuclear positioning [23, 38, 39]. Following serum starvation, monolayers of NIH 3T3 fibroblasts are wounded and stimulated with lysophosphatidic acid (LPA), which induces the movement of nuclei away from the wound edge [24]. This process is mediated by the retrograde flow of perinuclear actin cables, which are coupled to the nuclear envelope via linear arrays of LINC complexes [23, 40]. As previously shown, knockdown of either SUN2 or Nesprin-2 blocked rearward nuclear movements and centrosome orientation (Figure 6) [23]. The SUN2 and Nesprin-2 small interfering RNA (siRNA) defects were efficiently rescued by transient expression of EGFP-SUN2^{WT} or EGFP-mini-Nesprin-2G^{WT}, respectively (Figure 6) [23].

The siRNA rescue assays were used to test the importance of the predicted disulfide bond between SUN2 and Nesprin-2G. Mutating either conserved cysteine, in EGFP-SUN2^{C577S} or EGFP-mini-Nesprin-2G^{C-23S}, blocked the rescue of centrosome orientation (Figure 6B) and the rearward nuclear positioning defects (Figure 6C) caused by the depletion of SUN2 or Nesprin-2G, respectively. These results suggest that the ability of SUN2 to form an intermolecular disulfide bond with Nesprin-2G is critical for actin-mediated rearward nuclear positioning in migrating fibroblasts.

The Role of the Conserved Aromatic Residues at –7 of KASH Domains in the Presence of the Disulfide Bond

We next tested the extent to which conserved aromatic residues at −7 of KASH domains (Figure 1B) were required in the context of a longer KASH domain predicted to form disulfide bonds with SUN partners. Mutation of the phenylalanine at −7 in the ANC-1

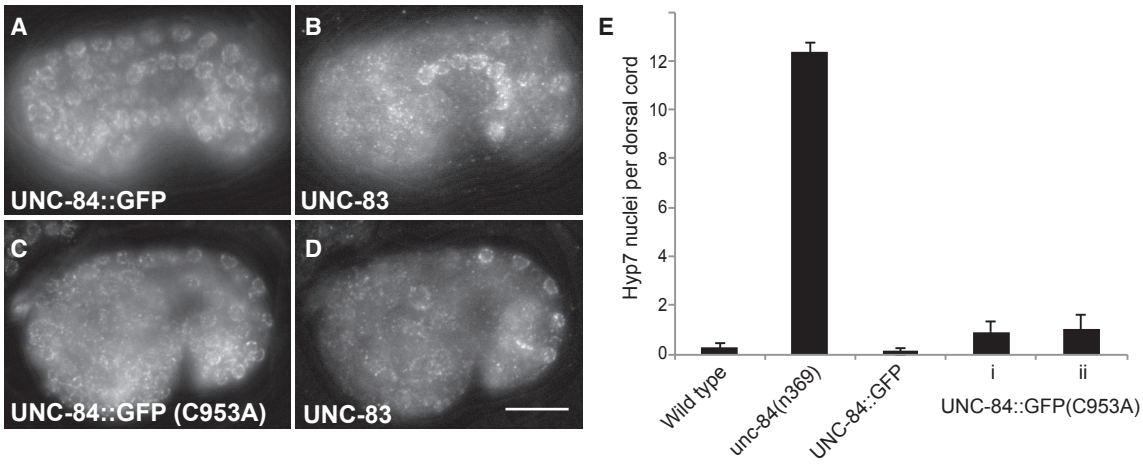

Figure 5. The Conserved Cysteine in UNC-84 Is Not Required for Nuclear Migration

(A–D) Anti-GFP (A and C) and anti-UNC-83 (B and D) immunolocalization in comma-stage embryos. Anterior is left; dorsal is up. Scale bar, 10 μm.

(E) Quantification of nuclear migration defects as in Figure 2. Error bars are 95% CI.

KASH domain did not cause a nuclear anchorage defect in adult *C. elegans* hypodermal cells; an average of 4.3% ± 1.2% (mean ± 95% CI) of hypodermal nuclei per lateral side of an animal were clustered (Figures 4G and 4H), which is not significantly different from the wild-type number of 2.4% ± 1.3% ($p = 0.058$ in a t test compared to wild-type). Thus, the presence of an intermolecular disulfide bond could at least partially compensate for a mutation in the KASH −7 aromatic residue in the UNC-84-ANC-1 interaction. In contrast, expression of an EGFP-mini-nesprin-2G construct harboring a mutation of the tyrosine at −7 in the KASH domain failed to rescue rearward nuclear positioning in nesprin-2-depleted NIH 3T3 fibroblasts during centrosome orientation (Figure 6). These results suggest that the conserved aromatic residues at the −7 position of KASH domains may be necessary for the transmission of forces generated by the actin cytoskeleton to move nuclei, whereas they are dispensable for resisting the forces experienced by nuclei anchored to the actin cytoskeleton in moving *C. elegans* animals. In agreement with this, our molecular dynamics results showed that despite the detachment of residues 0 to −17 in the KASH(Y-7A) mutation, the remaining residues (−18 to −23) remained intact due to the presence of the intermolecular disulfide bond (Figure 3).

Modeling Force Transfer across LINC Complexes by Molecular Dynamics

Our working model predicts that mechanical forces generated in the cytoskeleton are transferred across the nuclear envelope through LINC complexes and that disulfide bonds between SUN and KASH domains are important for the transfer of forces. We therefore modeled how SUN-KASH interactions would be affected with and without the disulfide bond. We used molecular dynamics to simulate constant-velocity pulling on the amino-terminal residue of the KASH peptide of human Nesprin-2 attached to SUN2 at a constant velocity of 0.05 m/s in wild-type (Figure 7A) and the SUN2 (C563A) mutation (Figure 7B). Each simulation was run three times. In a previous study, we applied tension on KASH domains by exerting a constant force on each KASH peptide [35]. As opposed to constant-force simulations, in this study, constant-velocity pulling was used and the changes in the magnitude of forces that the complex was able to withstand were extracted. In the SUN2 (C563A) mutation model, the KASH peptide begins to detach from the SUN protomer under virtually zero forces and both KASH peptides and the KASH lids of SUN domains are stretched to accommodate the pulling (Figures 7B and 7C). In contrast, the wild-type KASH peptide remains closely associated with the SUN trimer throughout the simulation, withstanding significantly higher forces, up to 250 pN ($N = 29{,}700$; $p < 0.0001$, obtained from a two-sample Kolmogorov-Smirnov test) (Figure 7C). Instead, the pulling forces are transferred past the SUN-KASH interaction and SUN domain and are relieved by stretching the coiled-coil domains (formed by α3) of SUN2 (Figures 7A, 7C, and 7D).

DISCUSSION

Interactions between conserved SUN and KASH domains form the core of the nuclear envelope-spanning LINC complex [3–5, 15, 41]. Here, we performed structural/functional analyses of the three interaction interfaces between SUN and KASH proteins. The C-terminal 4 residues of KASH proteins (0 to −3) interact with a binding pocket in SUN protomer P1, residues −4 to −14 interact with a cleft that is formed between the "KASH lid" of P1 and the core of the adjacent P2 protomer, and residues −15 to −23 interact with the surface of P2 [6]. We found that mutating any of the three interfaces disrupted the formation of LINC complexes and/or reduced the transfer of forces generated in the cytoplasm to the nucleoskeleton. Our results uncovered potential regulatory mechanisms for the formation and function of LINC complexes.

Mutational analysis of the two interfaces at the C terminus of KASH domains (consisting of KASH residues 0 to −14) showed they were necessary *in vivo* to move *C. elegans* hypodermal nuclei. These results are supported by the previous findings that the C-terminal 18 residues of the Nesprin-2 KASH domain are sufficient for binding SUN2 *in vitro* [6] and that the extension

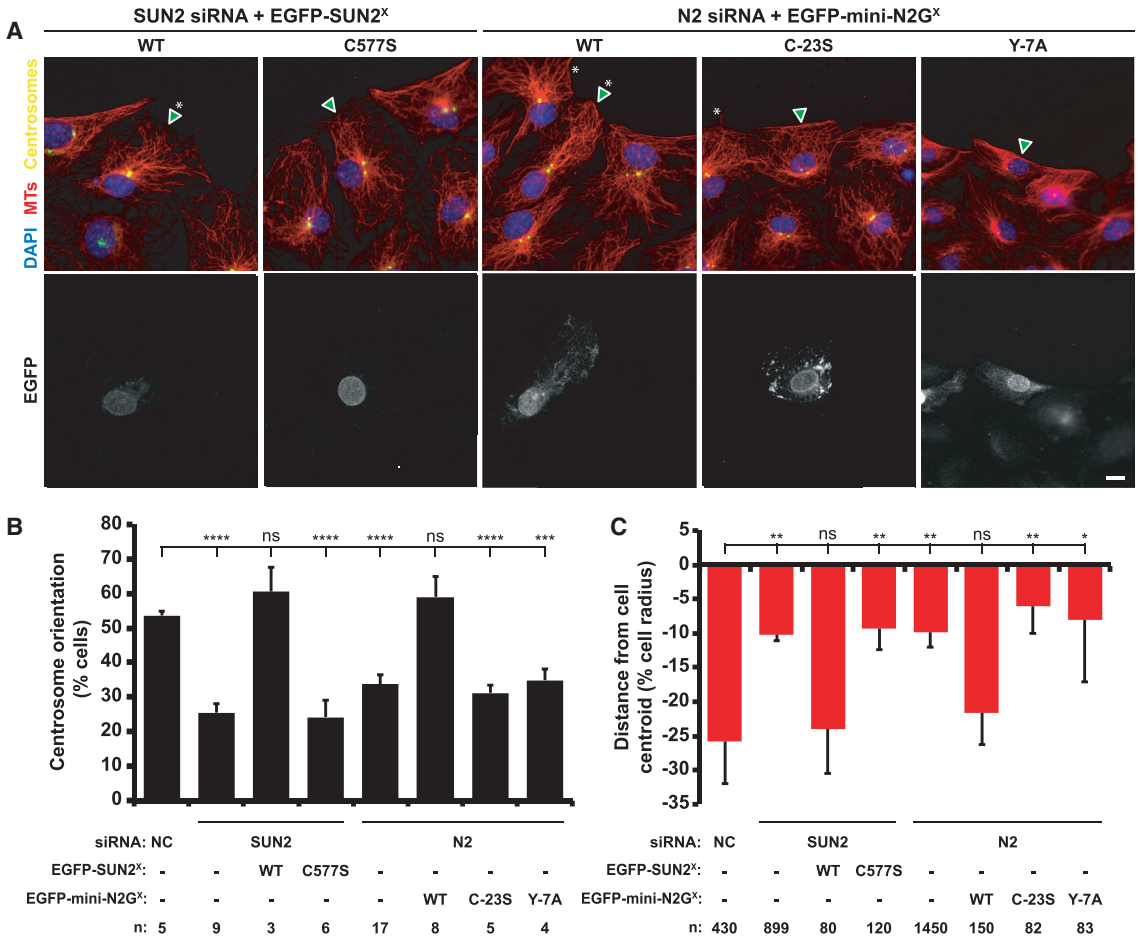

Figure 6. SUN2 C577 and Nesprin-2G C-23 Are Required for Rearward Nuclear Positioning during Centrosome Orientation

(A) Representative epifluorescence images of centrosome orientation in NIH 3T3 fibroblasts treated with siRNA and expressing the indicated cDNA constructs (arrowheads and bottom row of images). Asterisks, oriented centrosomes. Scale bar, 10 μm. MTs, microtubules.

(B) Centrosome orientation in the cells described in (A).

(C) Average nuclear positions from the cells described in (B). The cell center is defined as "0." Positive values are toward the leading edge, and negative values are away.

Two-tailed t tests were used to calculate p values (*p < 0.05, **p < 0.01, ***p < 0.001, ****p < 0.0001; ns, not significant). Error bars are 95% CI.

of the C terminus of KASH prevents its ability to interact with SUN2 *in vitro* [6, 33].

We also tested the extent to which the conserved aromatic residue at position −7 of KASH proteins functions in LINC assembly in our various experimental models and found significant differences. In *C. elegans* hyp7 precursors, UNC-83(Y-7A) expressed at endogenous levels localized to the nuclear envelope, but nuclear migration failed (Figures 3A–3E). These results suggest UNC-83(Y-7A) can weakly interact with UNC-84 at a level sufficient for localization to the nuclear envelope, but the interaction is unable to sustain the forces transferred across the LINC complex during nuclear migration. Our molecular dynamics simulations support this model. Without the tyrosine at position −7, KASH was unable to reach into the cleft between the two SUN protomers, resulting in the loss of several important interactions between the KASH tyrosine and a conserved motif on SUN (E552–S557 of SUN2; Figure 3). Likewise, the −7 tyrosine in the mouse nesprin-2G KASH domain was required for rearward nuclear migration and centrosome orientation in NIH 3T3 cells (Figure 6). In contrast, hypodermal syncytial nuclei were anchored normally in *anc-1(F-7A)* mutant animals. Perhaps the cysteine at −23 of KASH is sufficient to overcome the ANC-1(F-7A) mutation for nuclear anchorage, but both the −23 cysteine and the −7 tyrosine are required in NIH 3T3 cell rearward nuclear movements. Together, these findings suggest that the forces transmitted by LINC complexes required to move nuclei in polarizing fibroblasts may be greater than those required to anchor *C. elegans* hypodermal nuclei.

The third KASH-SUN interaction interface (−15 to −23) may solidify KASH-SUN complexes by forming an intermolecular disulfide bond between highly conserved cysteine residues in certain SUN and KASH pairs. Such a disulfide bond was observed between transiently expressed SUN and KASH proteins in HeLa cells [6]. We propose a model where the regulation of this third interface might enable a SUN protein homo-trimer to switch between different KASH proteins. In *C. elegans*, the SUN

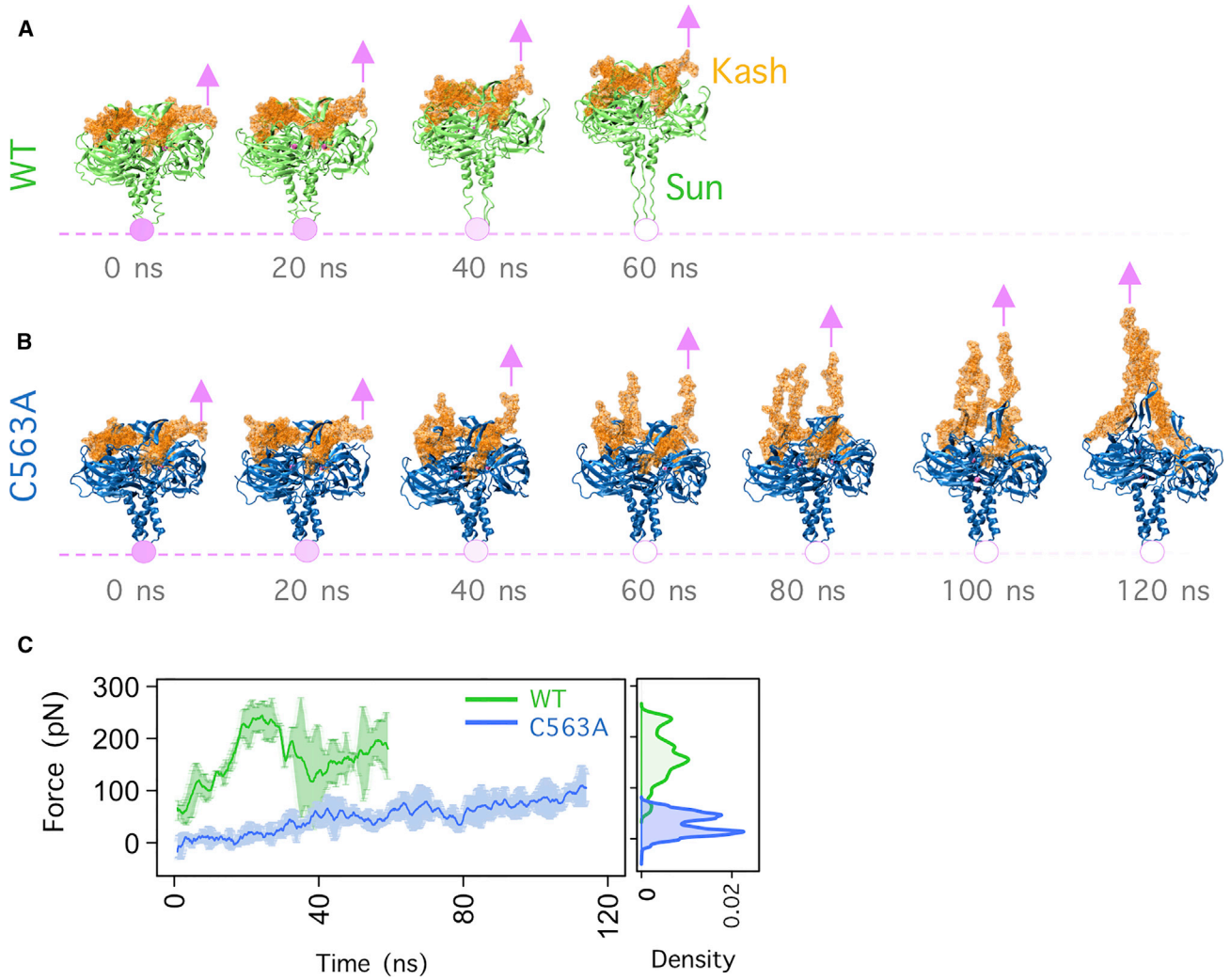

Figure 7. Modeling Force Transfer across LINC Complexes

(A and B) Snapshots of the trajectory of wild-type (A) and C563A (B) SUN2-KASH2 complexes under constant-velocity pulling. Pink arrows represent the location and direction of the applied constant velocity. Pink circles represent the fixed atoms.

(C) Forces on each KASH peptide required to displace the SUN-KASH complex at a constant velocity for wild-type (green) and C563A (blue) averaged over three molecular dynamics simulation runs. Error bars are the range. Right: a density plot shows the forces on each KASH peptide at each time point throughout the three simulations.

protein UNC-84 would first interact with the KASH protein UNC-83, which lacks the conserved cysteine, to move hypodermal nuclei. Then, UNC-84 would primarily interact with ANC-1 to anchor hypodermal nuclei. Because nuclear anchorage occurs over longer timescales, it might be advantageous to stabilize the UNC-84-ANC-1 interaction with a disulfide bond. The conserved cysteines in SUN2 and nesprin-2 were also necessary for actin-dependent rearward nuclear positioning during centrosome orientation in NIH 3T3 fibroblasts. In this manner, the rearward nuclear positioning in fibroblasts may be analogous to nuclear anchorage in the *C. elegans* hypodermis, as both processes use giant KASH proteins to tether nuclei to actin networks.

In further support of our proposed model for the role of an intermolecular disulfide bond in LINC complex function, molecular dynamics simulations suggested that the disulfide bond allows for maximal force transduction across the nuclear envelope. In the absence of a disulfide bond, constant pulling rapidly stretched KASH domains and the KASH lid of SUN domains. Only ~50 pN of force was transferred across the interface without the disulfide bond. In contrast, the presence of SUN-KASH intermolecular disulfide bonds transferred the forces on the KASH peptides directly to the coiled-coil trimerization domain in the luminal parts of SUN proteins while maintaining the stability of the SUN-KASH interface in our simulations. In this case, forces could be transferred across the LINC complex and ultimately to the nucleoskeleton and/or chromatin. These findings suggest that higher forces and/or a more stable interaction may be required to anchor nuclei to actin networks more permanently, versus the interactions to microtubules during *C. elegans* nuclear migration that are only required for brief

times. It is likely that other nuclear movements or other roles of LINC complexes in human development and disease will have a similar mode of regulation.

If the cell regulates the formation and reduction of the predicted SUN-KASH intermolecular disulfide bond, an interesting question is how it might do so. There are three protein disulfide isomerases in *C. elegans*. However, these three genes are understudied and their expression patterns could be developmentally regulated. A second possibility is that pulling across a disulfide bond could expose it to reduction [42]. Third, it has been proposed that the AAA+ ATPase Torsin could regulate the formation of LINC complexes [38, 43–45]. Future experiments could distinguish between these and other possible regulatory mechanisms.

The KASH domains in *C. elegans* UNC-83 and mammalian KASH5 are well conserved but significantly shorter than those in other KASH proteins. Nevertheless, both bind canonical SUN proteins UNC-84 in *C. elegans*, or SUN1 and SUN2 in mammals [7, 8, 15, 28]. UNC-83 and KASH5 are transiently required during development, whereas ANC-1 and the other Nesprins tend to play longer-term roles. For example, UNC-83 is required for a few specific nuclear migration events that take ~10–30 min during *C. elegans* development [26, 27]. After migration, nuclei remain anchored in place for days by way of the interaction of ANC-1 with the actin cytoskeleton [14]. Similarly, KASH5 only functions a short time during meiotic prophase I [28], whereas other Nesprins function just before and after this narrow window [4]. These findings suggest that evolution has maintained the disulfide bond in *C. elegans* and mammalian LINC complexes that function long term and/or require maximal force transduction but selected against the disulfide bond in LINC complexes that function transiently. The disulfide bond and third interaction domain may have been lost in KASH5 and UNC-83 after the divergence of nematodes, insects, and vertebrates, as both canonical KASH proteins in *Drosophila*, Klarsicht and MSP-300, have the conserved cysteine [5].

In summary, we have demonstrated here that all three interaction interfaces between conserved SUN and KASH proteins contribute to LINC complex function in nuclear positioning. Our findings from *C. elegans* development, mammalian cultured fibroblasts, and molecular dynamics simulations have led to a more complete mechanistic understanding of SUN-KASH interactions, which form the core of LINC complexes. Because LINC complexes are central to a multitude of cell and developmental functions and have been implicated in multiple pathologies [4, 5, 15, 46, 47], our mechanistic findings are likely to be important for understanding a variety of cell and developmental processes.

STAR★METHODS

Detailed methods are provided in the online version of this paper and include the following:

- KEY RESOURCES TABLE
- CONTACT FOR REAGENT AND RESOURCE SHARING
- EXPERIMENTAL MODEL AND SUBJECT DETAILS
- METHOD DETAILS
  - *C. elegans* CRISPR/Cas9 editing
  - Nuclear migration and anchorage assays in *C. elegans*
  - NIH 3T3 fibroblast manipulations
  - Immunofluorescence
  - Molecular Dynamics
- QUANTIFICATION AND STATISTICAL ANALYSIS

SUPPLEMENTAL INFORMATION

Supplemental Information includes one table and can be found with this article online at https://doi.org/10.1016/j.cub.2018.08.001.

ACKNOWLEDGMENTS

We thank Thomas Schwartz, Ulrike Kutay, and members of the Starr, Mofrad, and Luxton laboratories for helpful discussions. This work was supported by the NIH (R01GM073874 to D.A.S.; R21NS095109 to G.W.G.L.; and AR007612 to N.J.H.), National Science Foundation (CAREER award CBET-0955291 to M.R.K.M.), Natural Sciences and Engineering Research Council of Canada (to Z.J.), Dystonia Medical Research Foundation (to G.W.G.L.), and American Cancer Society Illinois Division (PF-13-094-01-CGC to N.E.C.).

AUTHOR CONTRIBUTIONS

Conceptualization, N.E.C., Z.J., M.R.K.M., G.W.G.L., and D.A.S.; Investigation, N.E.C., Z.J., A.S., V.A.V., B.E., H.H., N.J.H., L.A.H., and B.M.W.; Formal Analysis, all authors; Writing – Original Draft, N.E.C., Z.J., M.R.K.M., G.W.G.L., and D.A.S.; Writing – Review & Editing, all authors.

DECLARATION OF INTERESTS

N.E.C. is currently employed as a scientific editor at *Cell Reports*, which is a part of Cell Press.

Received: December 27, 2017
Revised: June 18, 2018
Accepted: August 1, 2018
Published: September 20, 2018

REFERENCES

1. Bone, C.R., and Starr, D.A. (2016). Nuclear migration events throughout development. J. Cell Sci. *129*, 1951–1961.
2. Gundersen, G.G., and Worman, H.J. (2013). Nuclear positioning. Cell *152*, 1376–1389.
3. Burke, B., and Roux, K.J. (2009). Nuclei take a position: managing nuclear location. Dev. Cell *17*, 587–597.
4. Ungricht, R., and Kutay, U. (2017). Mechanisms and functions of nuclear envelope remodelling. Nat. Rev. Mol. Cell Biol. *18*, 229–245.
5. Starr, D.A., and Fridolfsson, H.N. (2010). Interactions between nuclei and the cytoskeleton are mediated by SUN-KASH nuclear-envelope bridges. Annu. Rev. Cell Dev. Biol. *26*, 421–444.
6. Sosa, B.A., Rothballer, A., Kutay, U., and Schwartz, T.U. (2012). LINC complexes form by binding of three KASH peptides to domain interfaces of trimeric SUN proteins. Cell *149*, 1035–1047.
7. McGee, M.D., Rillo, R., Anderson, A.S., and Starr, D.A. (2006). UNC-83 is a KASH protein required for nuclear migration and is recruited to the outer nuclear membrane by a physical interaction with the SUN protein UNC-84. Mol. Biol. Cell *17*, 1790–1801.
8. Crisp, M., Liu, Q., Roux, K., Rattner, J.B., Shanahan, C., Burke, B., Stahl, P.D., and Hodzic, D. (2006). Coupling of the nucleus and cytoplasm: role of the LINC complex. J. Cell Biol. *172*, 41–53.
9. Haque, F., Lloyd, D.J., Smallwood, D.T., Dent, C.L., Shanahan, C.M., Fry, A.M., Trembath, R.C., and Shackleton, S. (2006). SUN1 interacts with nuclear lamin A and cytoplasmic nesprins to provide a physical connection between the nuclear lamina and the cytoskeleton. Mol. Cell. Biol. *26*, 3738–3751.

10. Padmakumar, V.C., Libotte, T., Lu, W., Zaim, H., Abraham, S., Noegel, A.A., Gotzmann, J., Foisner, R., and Karakesisoglou, I. (2005). The inner nuclear membrane protein Sun1 mediates the anchorage of Nesprin-2 to the nuclear envelope. J. Cell Sci. *118*, 3419–3430.
11. Malone, C.J., Fixsen, W.D., Horvitz, H.R., and Han, M. (1999). UNC-84 localizes to the nuclear envelope and is required for nuclear migration and anchoring during *C. elegans* development. Development *126*, 3171–3181.
12. Bone, C.R., Tapley, E.C., Gorjánácz, M., and Starr, D.A. (2014). The *Caenorhabditis elegans* SUN protein UNC-84 interacts with lamin to transfer forces from the cytoplasm to the nucleoskeleton during nuclear migration. Mol. Biol. Cell *25*, 2853–2865.
13. Rothballer, A., and Kutay, U. (2013). The diverse functional LINCs of the nuclear envelope to the cytoskeleton and chromatin. Chromosoma *122*, 415–429.
14. Starr, D.A., and Han, M. (2002). Role of ANC-1 in tethering nuclei to the actin cytoskeleton. Science *298*, 406–409.
15. Luxton, G.W.G., and Starr, D.A. (2014). KASHing up with the nucleus: novel functional roles of KASH proteins at the cytoplasmic surface of the nucleus. Curr. Opin. Cell Biol. *28*, 69–75.
16. Janota, C.S., Calero-Cuenca, F.J., Costa, J., and Gomes, E.R. (2017). SnapShot: nucleo-cytoskeletal interactions. Cell *169*, 970–970.e1.
17. Wang, W., Shi, Z., Jiao, S., Chen, C., Wang, H., Liu, G., Wang, Q., Zhao, Y., Greene, M.I., and Zhou, Z. (2012). Structural insights into SUN-KASH complexes across the nuclear envelope. Cell Res. *22*, 1440–1452.
18. Hennen, J., Hur, K.-H., Saunders, C.A., Luxton, G.W.G., and Mueller, J.D. (2017). Quantitative brightness analysis of protein oligomerization in the nuclear envelope. Biophys. J. *113*, 138–147.
19. Hennen, J., Saunders, C.A., Mueller, J.D., and Luxton, G.W.G. (2018). Fluorescence fluctuation spectroscopy reveals differential SUN protein oligomerization in living cells. Mol. Biol. Cell *29*, 1003–1011.
20. Sosa, B.A., Kutay, U., and Schwartz, T.U. (2013). Structural insights into LINC complexes. Curr. Opin. Struct. Biol. *23*, 285–291.
21. Zhou, K., and Hanna-Rose, W. (2010). Movers and shakers or anchored: *Caenorhabditis elegans* nuclei achieve it with KASH/SUN. Dev. Dyn. *239*, 1352–1364.
22. Starr, D.A., and Han, M. (2005). A genetic approach to study the role of nuclear envelope components in nuclear positioning. Novartis Found. Symp. *264*, 208–219, discussion 219–230.
23. Luxton, G.W.G., Gomes, E.R., Folker, E.S., Vintinner, E., and Gundersen, G.G. (2010). Linear arrays of nuclear envelope proteins harness retrograde actin flow for nuclear movement. Science *329*, 956–959.
24. Gomes, E.R., Jani, S., and Gundersen, G.G. (2005). Nuclear movement regulated by Cdc42, MRCK, myosin, and actin flow establishes MTOC polarization in migrating cells. Cell *121*, 451–463.
25. Chang, W., Antoku, S., and Gundersen, G.G. (2016). Wound-healing assays to study mechanisms of nuclear movement in fibroblasts and myoblasts. In Electron Microscopy Methods in Molecular Biology, S. Shackleton, P. Collsa, and E.C. Shirmer, eds. (Springer), pp. 255–267.
26. Fridolfsson, H.N., and Starr, D.A. (2010). Kinesin-1 and dynein at the nuclear envelope mediate the bidirectional migrations of nuclei. J. Cell Biol. *191*, 115–128.
27. Starr, D.A., Hermann, G.J., Malone, C.J., Fixsen, W., Priess, J.R., Horvitz, H.R., and Han, M. (2001). unc-83 encodes a novel component of the nuclear envelope and is essential for proper nuclear migration. Development *128*, 5039–5050.
28. Horn, H.F., Kim, D.I., Wright, G.D., Wong, E.S.M., Stewart, C.L., Burke, B., and Roux, K.J. (2013). A mammalian KASH domain protein coupling meiotic chromosomes to the cytoskeleton. J. Cell Biol. *202*, 1023–1039.
29. Roux, K.J., Crisp, M.L., Liu, Q., Kim, D., Kozlov, S., Stewart, C.L., and Burke, B. (2009). Nesprin 4 is an outer nuclear membrane protein that can induce kinesin-mediated cell polarization. Proc. Natl. Acad. Sci. USA *106*, 2194–2199.
30. Zhen, Y.-Y., Libotte, T., Munck, M., Noegel, A.A., and Korenbaum, E. (2002). NUANCE, a giant protein connecting the nucleus and actin cytoskeleton. J. Cell Sci. *115*, 3207–3222.
31. Zhang, Q., Skepper, J.N., Yang, F., Davies, J.D., Hegyi, L., Roberts, R.G., Weissberg, P.L., Ellis, J.A., and Shanahan, C.M. (2001). Nesprins: a novel family of spectrin-repeat-containing proteins that localize to the nuclear membrane in multiple tissues. J. Cell Sci. *114*, 4485–4498.
32. Zhang, X., Xu, R., Zhu, B., Yang, X., Ding, X., Duan, S., Xu, T., Zhuang, Y., and Han, M. (2007). Syne-1 and Syne-2 play crucial roles in myonuclear anchorage and motor neuron innervation. Development *134*, 901–908.
33. Stewart-Hutchinson, P.J., Hale, C.M., Wirtz, D., and Hodzic, D. (2008). Structural requirements for the assembly of LINC complexes and their function in cellular mechanical stiffness. Exp. Cell Res. *314*, 1892–1905.
34. Bone, C.R., Chang, Y.-T., Cain, N.E., Murphy, S.P., and Starr, D.A. (2016). Nuclei migrate through constricted spaces using microtubule motors and actin networks in *C. elegans* hypodermal cells. Development *143*, 4193–4202.
35. Jahed, Z., Shams, H., and Mofrad, M.R.K. (2015). A disulfide bond is required for the transmission of forces through SUN-KASH complexes. Biophys. J. *109*, 501–509.
36. D'Alessandro, M., Hnia, K., Gache, V., Koch, C., Gavriilidis, C., Rodriguez, D., Nicot, A.-S., Romero, N.B., Schwab, Y., Gomes, E., et al. (2015). Amphiphysin 2 orchestrates nucleus positioning and shape by linking the nuclear envelope to the actin and microtubule cytoskeleton. Dev. Cell *35*, 186–198.
37. Lawrence, K.S., Tapley, E.C., Cruz, V.E., Li, Q., Aung, K., Hart, K.C., Schwartz, T.U., Starr, D.A., and Engebrecht, J. (2016). LINC complexes promote homologous recombination in part through inhibition of nonhomologous end joining. J. Cell Biol. *215*, 801–821.
38. Saunders, C.A., Harris, N.J., Willey, P.T., Woolums, B.M., Wang, Y., McQuown, A.J., Schoenhofen, A., Worman, H.J., Dauer, W.T., Gundersen, G.G., and Luxton, G.W. (2017). TorsinA controls TAN line assembly and the retrograde flow of dorsal perinuclear actin cables during rearward nuclear movement. J. Cell Biol. *216*, 657–674.
39. Folker, E.S., Östlund, C., Luxton, G.W.G., Worman, H.J., and Gundersen, G.G. (2011). Lamin A variants that cause striated muscle disease are defective in anchoring transmembrane actin-associated nuclear lines for nuclear movement. Proc. Natl. Acad. Sci. USA *108*, 131–136.
40. Luxton, G.W.G., Gomes, E.R., Folker, E.S., Worman, H.J., and Gundersen, G.G. (2011). TAN lines: a novel nuclear envelope structure involved in nuclear positioning. Nucleus *2*, 173–181.
41. Razafsky, D., and Hodzic, D. (2009). Bringing KASH under the SUN: the many faces of nucleo-cytoskeletal connections. J. Cell Biol. *186*, 461–472.
42. Wiita, A.P., Ainavarapu, S.R.K., Huang, H.H., and Fernandez, J.M. (2006). Force-dependent chemical kinetics of disulfide bond reduction observed with single-molecule techniques. Proc. Natl. Acad. Sci. USA *103*, 7222–7227.
43. Starr, D.A., and Rose, L.S. (2017). TorsinA regulates the LINC to moving nuclei. J. Cell Biol. *216*, 543–545.
44. Gerace, L. (2004). TorsinA and torsion dystonia: unraveling the architecture of the nuclear envelope. Proc. Natl. Acad. Sci. USA *101*, 8839–8840.
45. Sosa, B.A., Demircioglu, F.E., Chen, J.Z., Ingram, J., Ploegh, H.L., and Schwartz, T.U. (2014). How lamina-associated polypeptide 1 (LAP1) activates Torsin. eLife *3*, e03239.
46. Calvi, A., and Burke, B. (2015). LINC Complexes and Their Role in Human Disease (John Wiley & Sons).
47. Cartwright, S., and Karakesisoglou, I. (2014). Nesprins in health and disease. Semin. Cell Dev. Biol. *29*, 169–179.
48. Cain, N.E., Tapley, E.C., McDonald, K.L., Cain, B.M., and Starr, D.A. (2014). The SUN protein UNC-84 is required only in force-bearing cells to maintain nuclear envelope architecture. J. Cell Biol. *206*, 163–172.
49. Brenner, S. (1974). The genetics of *Caenorhabditis elegans*. Genetics *77*, 71–94.

50. Dickinson, D.J., Ward, J.D., Reiner, D.J., and Goldstein, B. (2013). Engineering the *Caenorhabditis elegans* genome using Cas9-triggered homologous recombination. Nat. Methods *10*, 1028–1034.

51. Paix, A., Folkmann, A., Rasoloson, D., and Seydoux, G. (2015). High efficiency, homology-directed genome editing in *Caenorhabditis elegans* using CRISPR-Cas9 ribonucleoprotein complexes. Genetics *201*, 47–54.

52. Phillips, J.C., Braun, R., Wang, W., Gumbart, J., Tajkhorshid, E., Villa, E., Chipot, C., Skeel, R.D., Kalé, L., and Schulten, K. (2005). Scalable molecular dynamics with NAMD. J. Comput. Chem. *26*, 1781–1802.

53. Humphrey, W., Dalke, A., and Schulten, K. (1996). VMD: visual molecular dynamics. J. Mol. Graph. *14*, 33–38, 27–28.

54. Palazzo, A.F., Joseph, H.L., Chen, Y.J., Dujardin, D.L., Alberts, A.S., Pfister, K.K., Vallee, R.B., and Gundersen, G.G. (2001). Cdc42, dynein, and dynactin regulate MTOC reorientation independent of Rho-regulated microtubule stabilization. Curr. Biol. *11*, 1536–1541.

55. Dickinson, D.J., Pani, A.M., Heppert, J.K., Higgins, C.D., and Goldstein, B. (2015). Streamlined genome engineering with a self-excising drug selection cassette. Genetics *200*, 1035–1049.

56. Arribere, J.A., Bell, R.T., Fu, B.X.H., Artiles, K.L., Hartman, P.S., and Fire, A.Z. (2014). Efficient marker-free recovery of custom genetic modifications with CRISPR/Cas9 in *Caenorhabditis elegans*. Genetics *198*, 837–846.

57. Paix, A., Schmidt, H., and Seydoux, G. (2016). Cas9-assisted recombineering in *C. elegans*: genome editing using in vivo assembly of linear DNAs. Nucleic Acids Res. *44*, e128.

58. Richardson, C.D., Ray, G.J., DeWitt, M.A., Curie, G.L., and Corn, J.E. (2016). Enhancing homology-directed genome editing by catalytically active and inactive CRISPR-Cas9 using asymmetric donor DNA. Nat. Biotechnol. *34*, 339–344.

59. Liu, Z., Kirch, S., and Ambros, V. (1995). The *Caenorhabditis elegans* heterochronic gene pathway controls stage-specific transcription of collagen genes. Development *121*, 2471–2478.

STAR★METHODS

KEY RESOURCES TABLE

REAGENT or RESOURCE	SOURCE	IDENTIFIER
Antibodies		
mouse monoclonal anti-UNC-84	[48]	L72/6
mouse monoclonal anti-UNC-83	[27]	1209D7
rabbit polyclonal anti-GFP	Novus Biologicals	RRID:AB_10003058; NB600-308
mouse monoclonal anti-GFP	Clontech	RRID:AB_10013427; JL-8
rabbit polyclonal anti-pericentrin	Covance	RRID:AB_291635; PRB-432C
rat monoclonal anti-tyrosinated α-tubulin	European Collection of Animal Cultures	YL1/2
AlexaFluor secondary antibody 488 donkey anti-rabbit	Thermo Fisher	Cat#A-21206
AlexaFluor secondary antibody 555 goat anti-mouse	Thermo Fisher	Cat#A-21422
AlexaFluor secondary antibody 594 donkey anti-mouse	Thermo Fisher	Cat#R37115
Lipofectamine RNAiMAX	Thermo Fisher	Cat#13778075
Fluoromount-G	Thermo Fisher	Cat#00-4958-02
Bacterial and Virus Strains		
E. coli OP50	*Caenorhabditis* Genetics Center	N/A
Chemicals, Peptides, and Recombinant Proteins		
LPA	Avanti Polar Lipids	Cat#857130P
tetramisole	Sigma-Aldrich	Cat#L9756
Cas9 protein	QB3 UC Berkeley	N/A
Critical Commercial Assays		
Lipofectamine RNAiMAX	Thermo Fisher	Cat#13778150
Q5 Site-directed mutagenesis kit	New England Biolabs	Cat#E0554
Experimental Models: Cell Lines		
NIH 3T3 fibroblasts	ATCC	ATCC CRL-1658
Experimental Models: Organisms/Strains		
C. elegans strain: *wild type*	[49]	N2
C. elegans strain: *unc-84(n369)*	[11]	MT369
C. elegans strain: *unc-83(e1408)*	[27]	CB1408
C. elegans strain: *anc-1(e1873)*	[14]	CB3440
C. elegans strain: *unc-83(yc26[unc-83::gfp::kash + LoxP])V*	[34]	UD473
C. elegans strain: *unc-84(yc24[unc-84::gfp+LoxP])X*	[37]	UD476
C. elegans strain: *unc-19(ed3)I, yc28[unc-83::gfp::kash+A, LoxP::unc-19(+)::LoxP]V.*	this paper	UD478
C. elegans strain: *unc-84(yc35[unc-84(C953A)::gfp + LoxP])X*	this paper	UD497 & UD498
C. elegans strain: *anc-1(*yc48*[kash(CC,-24,-23,AA)]);dpy-10*	this paper	UD558
C. elegans strain: *unc-83(yc50[unc-83::gfp::kash(Y-7A) +LoxP])V*	this paper	UD568
C. elegans strain: *ycEx249[p_{col-19}::gfp::lacZ, p_{myo-2}::mCherry]*	this paper	UD522
C. elegans strain: *anc-1(yc56[F-7A]) I; ycEx249[p_{col-19}::gfp::lacZ, p_{myo-2}::mCherry]*	this paper	UD584
Oligonucleotides		
See Table S1	N/A	N/A
Recombinant DNA		
p_{eft-3}::*Cas9* + Empty sgRNA	gift from Bob Goldstein [50]	pDD162; Addgene plasmid # 47549
unc-83::gfp::kash homologous repair template	[34]	pSL718
unc-83::gfp::kash+A homologous repair template	this paper	pSL724

(*Continued on next page*)

Continued

REAGENT or RESOURCE	SOURCE	IDENTIFIER
Cas9 sgRNA construct for *unc-83* ctatgataattgtgtccac	[34]	pSL715
Cas9 sgRNA construct for *unc-84* gttgtgtcaacaagatgct	this study	pSL771
Cas9-sgRNA vector	gift from Geraldine Seydoux [51]	AP568-2; Addgene plasmid # 70047
promoterless *gfp::lacZ::nls* expression construct	gift from Andrew Fire	pPD96.04; Addgene plasmid #1502
$p_{col\text{-}19}$*::gfp::lacZ::nls* expression construct	this paper	pSL779
SUN2 siRNA rescuing construct	[23]	EGFP-SUN2^{WT}
SUN2 siRNA rescuing construct with C577S	this paper	EGFP-SUN2^{C577S}
Nesprin-2G siRNA rescuing construct	[23]	EGFP-mini-Nesprin-2^{WT}
Nesprin-2G siRNA rescuing construct with C-23S	this paper	EGFP-mini-Nesprin-2G$^{C\text{-}23S}$
$p_{myo\text{-}2}$*::mCherry*	gift from Erik Jorgensen	pCFJ90; Addgene plasmid # 19327
Software and Algorithms		
NAMD with CHARMM27 Molecular dynamics	[52]	http://www.ks.uiuc.edu/Development/Download/download.cgi?PackageName=NAMD
Langevin's piston and Hoover's method	[52]	N/A
VMD	[53]	http://www.ks.uiuc.edu/Development/Download/download.cgi?PackageName=VMD
LAS X Life Science	Leica	https://www.leica-microsystems.com/products/microscope-software/details/product/leica-las-x-ls/
NIS-Elements software	Nikon	https://www.nikoninstruments.com/Products/Software/NIS-Elements-Confocal/NIS-Elements-Viewer
ImageJ	NIH	https://imagej.nih.gov/ij/
R	The R Foundation	https://www.r-project.org/
Excel	Microsoft	https://products.office.com/en-US/excel

CONTACT FOR REAGENT AND RESOURCE SHARING

Further information and requests for resources and reagents should be directed to and will be fulfilled by the Lead Contact, Daniel A. Starr (dastarr@ucdavis.edu).

EXPERIMENTAL MODEL AND SUBJECT DETAILS

Caenorhabditis elegans were cultured on nematode growth medium plates spotted with OP50 bacteria and maintained at 15°C or room temperature (approximately 22°C). N2 was used as the wild-type control strain [49]. Some strains were provided by the *Caenorhabditis* Genetics Center, funded by the National Institutes of Health Office of Research Infrastructure Programs (P40 OD010440). Only healthy animals that were not used in previous procedures and were naive to testing were used. See the Key Resources Table for strain list.

Low-passage NIH 3T3 fibroblasts (authenticated by ATCC and of unknown sex) were cultured in DMEM with 10% bovine calf serum (Thermo Fischer). For polarization assays, cells were serum starved for 2 days, wounded and stimulated with 10 μM LPA (Avanti Polar Lipids) [24, 54]. Cells were grown at 37°C in 5% CO_2.

METHOD DETAILS

C. elegans CRISPR/Cas9 editing

Knock-in strains were constructed using CRISPR/Cas9-mediated genome editing [50, 55–57]. Some Cas9 targeting sequences were cloned into pDD162 ($p_{eft\text{-}3}$*::Cas9* + Empty sgRNA, a gift from Bob Goldstein, Addgene plasmid # 47549) [50], using Q5 site-directed mutagenesis (New England Biolabs). For others, guideRNAs were synthesized and pre-complexed with purified Cas9 protein. Targeting sequences for each strain are listed in Table S1.

unc-83::gfp::kash(+A) was generated using *unc-19(ed3)* rescue [34, 50]. An alanine codon was inserted before the stop into pSL718 [34] using Q5 site-directed mutagenesis to create the homologous repair template pSL724, which was used with

Cas9-sgRNA construct pSL715 and injection markers as reported [50] to make UD478: *unc-19(ed3)I, yc28[unc-83::gfp::kash+A, LoxP::unc-19(+)::LoxP]V*.

The *unc-84::gfp(C953A)* mutation was introduced into *unc-84::gfp* (UD476) by CRISPR co-conversion with single stranded oligodeoxyribonucleotide repair templates containing *unc-84(C953A)* and *dpy-10(cn64)* [51, 56], using Cas9-sgRNA constructs pSL771 and AP568-2 (gift from Geraldine Seydoux, Addgene plasmid #70047) [51]. Two independent integrated lines were isolated and analyzed UD497 and UC498: *yc35[unc-84(C953A)::gfp + LoxP]X.*

The *anc-1(yc48)*, *anc-1(yc56)*, and *unc-83(yc50)* mutations were made by directly injecting RNA/Cas9 complexes into *C. elegans* gonads [56–58]. To make *anc-1(yc48)*, 17.5 μM of pre-complexed Alt-R CRISPR *anc-1* crRNA #1 (synthesized by Integrated DNA technologies, see Table S1), tracrRNA (Integrated DNA Technologies), and Cas9 purified protein (QB3 Berkeley) were injected with 6 μM ssDNA repair templates (Integrated DNA Technologies, see Table S1). *anc-1(yc48)* mutates cysteine residues at −23 and −24 of the KASH domain to alanines to make ANC-1(CC-23-24AA) in strain UD558. To make *unc-83(yc50)* and *anc-1(yc56)*, 4 μg crRNA against *unc-83* or crRNA #2 against *anc-1*, 1.25 μg crRNA against *dpy-10*, 10 μg tracrRNA (Dharmacon), 25 μg of Cas9 protein, 1.1 μg ssDNA repair template (See Table S1), and 0.15 μg ssDNA repair for *dpy-10* in a total of 10 μL was injected into young adult gonads [57]. *unc-83(yc50)* mutates the conserved tyrosine at residue 967 of UNC-83 to make UNC-83(Y-7A) in strain UD568. *anc-1(yc56)* mutates the conserved phenylalanine at position −7 from the C terminus of ANC-1 to make ANC-1(F-7A).

A fluorescent marker to identify hypodermal nuclei in the adult animal was constructed by insertion of a 1 kb fragment upstream of the *col-19* gene [59] into pPD96.04 (gift from Andrew Fire, Addgene plasmid #1502) to create $p_{col\text{-}19}$*::gfp::lacZ* (pSL779). N2 animals were injected with pSL779 at 40 ng/μl, pBluescript SK+ at 50ng/μl, and pCFJ90 at 2 ng/μl to make strain UD522: *ycEx249[*$p_{col\text{-}19}$*::gfp::lacZ,* $p_{myo\text{-}2}$*::mCherry].* Transgenic animals were identified by red fluorescent pharynx in larval stages. Green hypodermal nuclei were observed in transgenic animals beginning at the L4 molt. The marker was introduced into other strains by crossing to UD522 transgenic males.

Nuclear migration and anchorage assays in *C. elegans*

Defects in hyp7 nuclear migration were quantified by counting the number of hyp7 nuclei found abnormally, using Nomarski optics, in the dorsal cords of L1 or L2 hermaphrodites. We scored all the hyp7 nuclei abnormally in the dorsal cord between the second bulb of the pharynx and the anus [12, 27]. Hyp7 nuclear clustering was assayed in adult animals expressing $p_{col\text{-}19}$*::gfp::lacZ*. Young adult hermaphrodites were mounted on 2% agarose pads with 10 mM tetramisole in M9 buffer. Nuclei were counted as clustered if within 10% nuclear diameter proximity to another nucleus in the same focal plane along the longitudinal axis of the worm, as determined by DIC microscopy. Contacts between nuclei on the perpendicular axis were not counted, as the marker could not distinguish seam cell nuclei in proximity to hyp7 nuclei from clusters of hyp7 nuclei. Only nuclei situated between the pharynx and the anus were counted, as nuclei near the mouth and at the very end of the tail were observed to cluster in wild-type animals. Only one lateral side of each animal was scored.

For both the nuclear migration and anchorage assays, *C. elegans* animals of the appropriate age were randomly selected at the dissecting microscope for scoring using the compound microscope and all scorable animals on the slide were counted. Animals were only scored if the entire animal was easily viewable. Although the genotypes were not blinded, animals from multiple plates were included in the datasets. In one case, the *unc-84::gfp(C953A)* mutant, two independently generated lines were assayed.

NIH 3T3 fibroblast manipulations

siRNA experiments were performed using 50nM siRNA duplexes (Shanghai GenePharma), which were transfected using Lipofectamine RNAiMAX (Thermo Fisher). The noncoding, Nesprin-2G, and SUN2 siRNA sequences were previously validated and listed in Table S1 [23]. EGFP-SUN2^{C577S} was made by *in vitro* mutagenesis of EGFP-SUN2^{WT} [23]. EGFP-mini-Nesprin-2G$^{C\text{-}23S}$ was similarly generated from EGFP-mini-Nesprin-2^{WT} [23]. The primers used to generate these constructs are in Table S1. Purified plasmid DNA was microinjected into NIH 3T3 cell nuclei at concentrations between 5 and 30 μg/mL [38]. Injections were performed on a TS100 microscope (Nikon) equipped with a chrome-free infinity Apochromat long working distance apodized dark low 20Å∼/NA 0.4 objective (3-mm working distance) and a Narishige NT-88 β [27, 48].

Immunofluorescence

For *C. elegans* experiments: Anti-UNC-84 mouse monoclonal antibody L72/6 [48] was used at 1:100 dilution. Mouse monoclonal anti-UNC-83 antibody 1209D7 [27] was used undiluted. Rabbit polyclonal anti-GFP antibody NB600-308 (Novus Biologicals) was used at 1:500 dilution. AlexaFluor secondary antibodies 488 donkey anti-rabbit, 555 goat anti-mouse, and 594 donkey anti-mouse (Thermo Fisher) were used at 1:500 dilution. Images were captured with a HCX Plan Apochromat 63, 1.40 NA objective on a compound microscope (DM6000) with LAS X software. Images were uniformly enhanced using the background subtraction and brightness/contrast commands in ImageJ.

For experiments with NIH 3T3 cells: NIH 3T3 fibroblasts were cultured in DMEM with 10% bovine calf serum (Thermo Fischer Scientific) on number 1.5 coverslips. Fibroblasts were serum starved for 2 d, wounded, and stimulated with 10 μM LPA for 2 hr before being fixed in in −20° methanol for 10 min. The fixed cells were then stained as follows. Anti-EGFP mouse monoclonal antibody JL-8 (Clontech) was used at a 1:200 dilution, anti-percentrin rabbit polyclonal antibody PRB-432C (Covance) was used at 1:200 dilution. Anti-tyrosinated α-tubulin rat monoclonal antibody YL1/2 (supernatant collected from hybridomas purchased from the European Collection of Animal Cell Cultures, Salisbury, UK) was used at 1:50 dilution. Goat anti-mouse, -rabbit, and -rat secondary antibodies

conjugated to AlexaFluor488, AlexaFluor555, AlexaFluor594, AlexaFluor650 (Thermo Fisher) were used at 1:200 dilution. Stained cells were mounted on slides using Fluoromount (Thermo Fisher).

Images were obtained with a Nikon Eclipse Ni-E microscope driven by NIS-Elements software using a Nikon oil immersion 40Å~/1.30 NA Plan Fluor Eco-Glass oil immersion objective lens (0.20-mm working distance), a Lumencor SOLA solid state white-light excitation subsystem, and a Photometrics CoolSNAP ES2 12-bit 20-MHz digital monochrome charge-coupled device camera. A custom DAPI filter for the SOLA light source was used, which consisted of an ET 395/25Å~excitation filter and an ET 460/50-m emission filter purchased from Chroma Technology Corp (Bellows Falls, VT). EGFP (C-FL EGFP hard coat high signal to noise Zero Shift; Nikon), Texas Red (C-FL Texas Red hard coat high signal to noise Zero Shift; Nikon), and Cy5 (C-FL CY5 hard coat high signal to noise Zero Shift; Nikon) filter sets were also used.

To quantify centrosome orientation, a fibroblast is divided by drawing a "v" that begins and ends at the left- and rightmost wound-edge, respectively. The middle of the "v" is defined by the center of the nucleus. The cell is scored as having an oriented centrosome if the centrosome resides within the "v" between the nucleus and the wound-edge. Since the "v" occupies ~1/3 of the cell, ~33% of wound-edge cells will have an oriented centrosome. Experiments were repeated at least 3 times.

To quantify nuclear positioning, fluorescence images of the stained cells described above were pseudocolored, combined and aligned such that the wound-edge was parallel to the x axis using ImageJ. Custom-made MATLAB software (MathWorks, Natick, MA) was then used to calculate the cell centroid and equivalent radius of the wound-edge cells, which were outlined by hand. Segmentation was used to identify the centroid of the nucleus and therefore the position of the organelle. A vector representing the distance from the nuclear centroid to the cell centroid was drawn and resolved into x and y coordinates (parallel and perpendicular to the leading edge, respectively). Measurements were normalized to cell size to allow for comparison between cells. Only the y-coordinate was used in plots as the x-coordinate (position of the nuclear centroid or centrosome along the x axis) did not change significantly. The difference between the cell centroid and the nucleus centroid or centrosome was then divided by the radius to determine the percentage of the cell radius the nucleus traveled.

Regarding the wounded fibroblast monolayer assay for rearward nuclear positioning during centrosome orientation, at least three independent biological replicates were performed and analyzed for each experiment. To compensate for the lack of blinding, five images of at least eighty cells were collected from three different wounds and all of the scorable wound edge cells were analyzed for the non-injected control experiments. For the injected experiments, all of the scorable EGFP-positive wound edge cells were analyzed. Cells were deemed unscorable if they were not entirely visualized within the field of view of an image.

Molecular Dynamics

All molecular dynamics simulations were performed with NAMD using the CHARMM27 force field [52] and visualized using VMD software [53]. The crystal structure used in these simulations was obtained from the protein data bank (PDB ID: 4DXS). Mutations were introduced using the VMD mutator plugin. All modeled structures were then solvated in water and an ion concentration of 150 mM of KCl and 50 μM of $CaCl_2$ was added to each system. Next, periodic boundary conditions were applied in all three directions and the systems were minimized for 5000 steps and equilibrated for ~3ns at 1 atm and 310 K using Langevin's piston and Hoover's method [52], For constant velocity pulling experiments, we attached a dummy atom to the position of the center of mass of the amino-terminal residue of the KASH peptide (C-23) via a virtual spring and fixed the C-terminal residue of SUN2. We then measured the forces between the dummy atom and C-23 using NAMD [52] as the dummy atom was moved at a constant velocity of 0.05 m/s.

QUANTIFICATION AND STATISTICAL ANALYSIS

The *C. elegans* nuclear migration and anchorage data in Figures 2, 3, 4, 5, and 6 are displayed as means with 95% CI as error bars; t tests were performed on indicated comparisons and the sample sizes were at least 20. For Figure 6 pertaining to the NIH 3T3 cells, sample sizes are indicated within the figure. Molecular dynamic simulations were performed in triplicate, plots were prepared using R software. The mean and range of data are shown in Figure 7C. A two-sample Kolmogorov-Smirnov test was performed to determine whether the observed difference in average forces obtained from molecular dynamics simulations is significantly lower in C563A versus wild-type. This test was conducted using the ks.test function in R *stats* package.